JOURNAL OF SOLID STATE CHEMISTRY **126,** 108–120 (1996)
ARTICLE NO. 0318

Ordering, Incommensuration, and Phase Transitions in Pyrrhotite

Part II: A High-Temperature X-Ray Powder Diffraction and Thermomagnetic Study

Fan Li and Hugo F. Franzen[1]

Ames Laboratory and Department of Chemistry, Iowa State University, Ames, Iowa 50011

Received April 8, 1996; in revised form June 17, 1996; accepted June 24, 1996

High-temperature X-ray diffraction (HTXRD) has been combined with thermomagnetic measurements to study synthetic and natural pyrrhotites. The temperature dependence of the properties observed in DTA, thermomagnetic and diffraction measurements indicates that transitions consistently occur upon heating and cooling so long as the sample is kept below 400°C, but if the ultimate heating temperature is higher than 550°C the transitions are altered, probably due to the loss of sulfur. The previously proposed transition sequence for Fe_7S_8 was supported by HTXRD observation, especially on natural monoclinic pyrrhotite. For intermediate pyrrhotite, the principal ordering was found to be the formation of Kagome nets, and it was found that the vertical stacking sequences that are commensurate along the *c* axis yield antiferromagnetic characteristics. Based on the changes observed in the HTXRD patterns it is proposed that the mechanism for an observed magnetic λ-transition between the temperatures 150 and 250°C is the transformation of a commensurate structure with *ABCD* layering of Kagome nets into a vacancy-disordered structure with the same *c* modulation.

1. INTRODUCTION

Studies of vacancy and magnetic spin orderings have been of special importance in solid state research because they lead directly to an understanding of crystallographic and magnetic structures. Nonetheless, two complications make such studies difficult: First, there is no method to directly probe the individual vacancies and magnetic spins. The macroscopic observations are averages over correlations among the vacancies and spins. Second, because the temperature, cooling rate, and other factors usually influence the resultant ordering, it is difficult to achieve nearly perfect ordering in a crystal. Different experimental conditions often alter the ordering path during property measurements. Thus it is frequently necessary for either thermodynamic or kinetic reasons to study an imperfect or incomplete ordering process.

Pyrrhotites, which are iron sulfides with the general composition $Fe_{1-x}S$ (x = 0–0.125), are typical defect compounds. The prototypical structure for this system is NiAs-like with antiferromagnetically coupled iron layers. At low temperature (below 400°C) most pyrrhotites exhibit some degree of superstructure development as the result of vacancy ordering, which, in turn, results in varied magnetic, thermal, and electric properties and complicated phase relations.

In previous studies (1–2), we have discussed the structural aspects and phase transitions for the two extreme cases of pyrrhotite, FeS and Fe_7S_8. In the FeS case, the transition sequence along the temperature scale is concluded to be: distorted troilite (antiferromagnetic with spins $\parallel$ **c**) $\rightarrow$ troilite (spins rotated to $\perp$**c**) $\rightarrow$ NiAs-type (paramagnetic with random spins). We have found that this transition sequence can be extended to the composition range, at least, from $Fe_{1.002}S$ to $Fe_{0.996}S$. When x reaches 0.05, pyrrhotite comes into a two-phase region where the troilite phase coexists with a hexagonal phase. The α transition for this region does not reverse upon cooling at the usual laboratory rates due to a transition collapse (3), and intermediate hexagonal phases result. In the Fe_7S_8 case, a perfect ordered structure can be achieved by the maximum separation of iron vacancy sites. This ordered structure has a stacking sequence of iron layers, as in the ideal model proposed by Bertaut (4), of D_AFD_BF D_CFD_DF along the c axis of the NiAs structural type (F stands for the iron filled layer; D_A, D_B, D_C, and D_D stand for the four Kagome nets unequivalent with respect to the origin). Based on the results of a TEM investigation, the idealized transition sequence was found to be: monoclinic *ABCD* stacking (ferrimagnetic) $\rightarrow$ trigonal *ABC* stacking (ferrimagnetic) $\rightarrow$ hexagonal structure with vacancies disordered within alternate planes (paramagnetic) $\rightarrow$ NiAs-type structure with disordered vacancies.

On the other hand, the pyrrhotites with intermediate compositions (x = 0.05–0.12) have also received considerable attention because this composition range is widely found among the natural pyrrhotite minerals, and because

0022-4596/96 $18.00

the order–disorder processes in this group of pyrrhotites remain unexplained. The main efforts regarding this composition range have focused on the following aspects:

1. Possible discrete phases. A number of stable *NC* superstructures (*A* and *C* are the axial lengths of the NiAs-type unit cell, and *N* is an integer) have been discovered by powder X-ray and electron diffraction experiments, such as 5*C* for Fe_9S_{10} (5), 6*C* for $Fe_{11}S_{12}$ (6), and 11*C* for $Fe_{10}S_{11}$ (7, 8). Their structures are generally based on the Fe_7S_8 structure, i.e., partially filled Kagome net layers and iron-filled layers that are stacked in such a way that long-range ordering is established along the *c* dimension, and these structures commonly have 2*A* repeats (inherent in Kagome nets) within the planes. Although these idealized superstructure types are theoretically possible, there is still a lack of evidence concerning structural details and information concerning transition sequences. On the other hand, evidence has revealed that some pyrrhotites over this composition range have hexagonal structures which have, in fact, integral $A_{\text{NiAs-type}}$ repeats but nonintegral $C_{\text{NiAs-type}}$ repeats. Apparently, this implies that incommensurate ordering also occurs in this system.

2. Magnetic properties. The magnetic behavior of pyrrhotite is sensitively altered by changes of composition. In addition to the antiferromagnetism found in stoichiometric or near stoichiometric iron sulfide ($Fe_{0.92}S$–FeS), other magnetic behaviors have been discovered and were categorized according to the following three types (9): (1) Weiss-type, that is, ferrimagnetic. This behavior corresponds to the composition ranging from $Fe_{0.87}S$ to $Fe_{0.88}S$, including Fe_7S_8. It has been widely accepted that this ferrimagnetism arises from unbalanced antiferromagnetic coupling, and that the Curie transition takes place at 315°C. (2) Peak-type, i.e., a so-called anti-Curie transition (because ferrimagnetism disappears as the temperature decreases) or a λ transition (because of the peak shape). The pyrrhotites showing this behavior have compositions between $Fe_{0.91}S$ and $Fe_{0.92}S$. In this case the magnetization is characterized by an abrupt rise and fall of a ferrimagnetic peak in a narrow temperature range (from 200 to 250°C), while elsewhere the pyrrhotite is antiferromagnetic. (3) Mixed-type. The pyrrhotite for this magnetic type is actually a mixture of Weiss-type and peak-type pyrrhotite, and hence the thermomagnetic behavior is a combination of the first two types.

Nevertheless, the mechanism of the anti-Curie transition has remained unexplained, even though the later discovery of the various *NC* superstructures seems to shed further light on the mechanism giving rise to its formation. One hypothesis proposed by Lotgering (10, 11) considered a competition between vacancy ordering and spin ordering. Since the spin ordering is a second-order transition but vacancy ordering is first order, Lotgering argued that it was possible for the free energy of a magnetically ordered but vacancy disordered phase to be less than that of a magnetically and vacancy ordered phase at some temperature below the Curie point. Thus the transition was proposed to be: a phase with ordered spins and disordered vacancies at the Néel point (315°C) $\xrightarrow{300°C}$ spins disordered and vacancies ordered $\xrightarrow{265°C}$ vacancies disordered and spins ordered (gradually to reach the maximum ferrimagnetization) → vacancy disordering at low temperature. This competitive ordering mechanism was not supported by the neutron diffraction experiments later conducted by Sparks *et al.* and Andersen *et al.* (12, 13). Another interpretation was proposed by Hirone *et al.* (14, 15). They suggested that there may be two vacancy-ordered phases, one that is ferrimagnetic stable at higher temperature, and the other, stable at lower temperature, is antiferromagnetic, and that they transform at T_λ (220°C). Since the magnetic transition occurs at about 280°C on a cooling ramp, rather than at 315°C at which temperature the spin ordering is supposed to occur, an extra vacancy disordered structure was proposed to follow the high-temperature ferrimagnetic structure. However, the DSC experiment carried out by the same authors revealed only two transitions at 220 and 315°C, instead of three transitions, and there was no experimental evidence to identify the two phases with different orderings on either side of T_λ. On the other hand, detailed thermodynamic data for the anti-Curie transition were acquired by Townsend's group (16). However, from the structural information obtained using Mossbauer spectroscopy at high temperature, they have not succeeded in identifying the structure that supports the ferrimagnetic superlattice over the temperature range 150–250°C. Therefore, an inherent relationship between the revealed *NC* superstructures and anti-Curie transition has not yet been established.

In the present work, we have performed high-temperature XRD, thermomagnetic, and DTA measurements on pyrrhotites with a variety of compositions with special attention paid to the intermediate pyrrhotites. These studies provide new insight into the phase relations in this system.

2. EXPERIMENTAL

All the pyrrhotite samples with compositions ranging between Fe/S = 1 : 1 and 0.875 were synthesized from pure elements sealed in evacuated silica glass tubes. The annealing procedures have been reported in previous papers (1, 2). The accurate compositions in the resultant samples were verified using an electron microprobe (EMP). At least 30 spots on an area of about 5 mm × 5 mm were analyzed for each sample. The standard deviation of the measured stoichiometry was lower than 1%. Besides the synthetic samples, naturally occurring pyrrhotites provided

TABLE 1
Description of the Natural Pyrrhotites Obtained from Inco

Name of sample	Inco 1	Inco 2	Inco 3	Inco 4
Source of product	mag. concentrates after mag. separation	nonmagnetic concentrates after mag. separation	fast flotation portion in floating separation from Inco2	slow flotation portion in floating separation from Inco2

by Inco Limited, Canada, were also studied. The samples were shipped in a slurry form. In order to dry the samples in our laboratory, they were heated at 100–120°C in glass tubes under pure N_2 (g). The descriptions of these natural samples are summarized in Table 1.

A high-temperature X-ray diffractometer (HTXRD) and a DTA apparatus were used as described previously (1, 2). The diffractometer was equipped with a Cr-anode source and a gas-flow proportional curved position sensitive detector (Inel CPS120). With these features a satisfactory pattern can be obtained within 10–20 min of collection time. The lowest angle of 2θ at which the detector can collect is 15° and the 2θ resolution can reach 0.015°. The samples for the HTXRD experiment were ground into very fine powder and loaded in a Ta-holder, to the bottom of which a chromel–alumel thermocouple was spot-welded. All the HTXRD measurements were performed under a vacuum of $\sim 10^{-4}$ Torr. In DTA measurements, the heating and cooling rates were 5 K/min under an Ar-gas flow with O_2 impurity <40 ppm. The differential temperature (ΔT) shown in the DTA figures has been consistently expressed in the degrees per milligram of sample. The thermal magnetization measurements were carried out using a vibrating sample magnetometer (VSM 4500, EG&G). The samples were accurately weighed and loaded into a BN_3 sample holder. The applied magnetic field was between 1500 and 22,000 Oe, depending on the magnetization of the sample. A pure argon atmosphere with O_2 impurity <40 ppm was maintained in the sample cylinder during the measurement.

3. RESULTS AND DISCUSSION

3.1. *Thermomagnetic Behaviors*

The thermomagnetic measurements on our synthesized samples demonstrated all three types of magnetic behavior described in the Introduction. Figures 1, 2, and 3 display Weiss-type curve from an Fe_7S_8 sample, the peak-type curve from an $Fe_{0.906}S$ sample, and a mixed-type curve from an $Fe_{0.887}S$ sample, respectively. Notice that since some of the samples contain traces of magnetite (by weight about 0–1.5%) formed during synthesis, the magnetization curves in the figures show a contribution from magnetite as demonstrated by its characteristic Curie transition (= 585°C). Nevertheless, some important features were observed and are summarized as follows:

(1) Saturation magnetization. For Fe_7S_8, the saturated magnetization can be reached when the external field exceeds 10,000 Oe (M = 15.9 emu/g at 20,000 Oe). However, the atomic magnetic moment could not be directly determined because of the anisotropy in polycrystalline pyrrhotite. In order to estimate the corrected saturation magnetization, a comparative experiment was carried out on a polycrystalline magnetite (Fe_3O_4) sample. The result showed that for Fe_3O_4 the experimental magnetization was 78% of that calculated. Hence the saturation magnetization for Fe_7S_8 was estimated to be 20.4 emu/g at room temperature, corresponding to a net magnetic moment J = 9.5 m_B per unit cell (a 4C structure containing four Fe_7S_8). This magnitude, though in a good agreement with the values measured by Schwarz and Hayase *et al.* (9, 17), is still

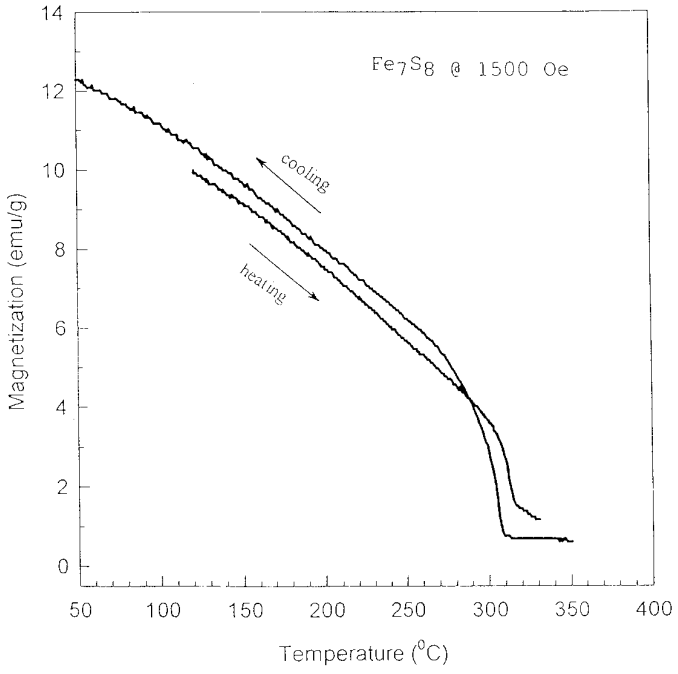

FIG. 1. Temperature dependence of magnetization for a Weiss-type pyrrhotite (Fe_7S_8).

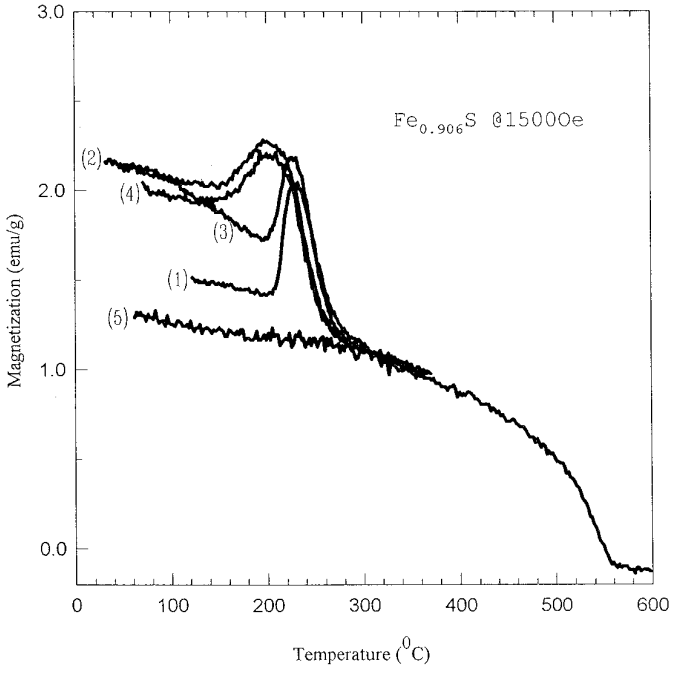

FIG. 2. Temperature dependence of magnetization for a peak-type pyrrhotite subjected to three sequential heating–cooling cycles: curve 1, heating from 120 to 350°C; curve 2, cooling from 350 to 30°C; curve 3, heating from 100 to 350°C; curve 4, cooling from 350 to 70°C; curve 5, cooling from 600 to 50°C. Notice that on curve 5 only the magnetization contributed by magnetite was maintained when the sample was cooled from 600°C.

less than that calculated according to Bertaut's model. Ideally, if all the spontaneous spins are assumed to lie exactly in the *a*–*b* plane and the antiferromagnetic coupling occurs only between the iron-filled layers and the iron-deficient layers, the net uncompensated moment will be 17.1 m_B per unit cell (according to $J = 4$ m_B for Fe^{++} and $J = 5$ m_B for Fe^{+++}). Accordingly, approximately 56% of the iron vacancies yield a net ferrimagnetism. Apparently, this analysis is valid even if Fe_7S_8 adopts the 3*C* structure because of the same vacancy density in both 4*C* and 3*C* structures and the magnetic configuration consisting of ferromagnetic coupling within the iron layers and antiferromagnetic coupling between the layers. In other words, out of the possible 1/8 of the vacant iron sites that could be uncompensated (assuming parallel ordered spins in the plane), only 57% contribute to the net ferrimagnetization, indicating that residual disorder or other factors such as canting of magnetic moment off the *c* plane have to be taken into account. As for the $Fe_{0.906}S$ sample, the maximum ferrimagnetization at the anti-Curie transition point is estimated to be approximately 1/5 of that in Fe_7S_8. This magnitude is compatible with the proportion of iron vacancies because cancellation of ferrimagnetism between the defect layers inevitably exists for this case.

(2) Magnetic reversibility. In the temperature range between 20 and 400°C, the thermomagnetic behavior for all the samples can be reversed upon change from heating to cooling. The ferrimagnetization in Weiss-type pyrrhotite was recovered with a hysteresis of 10–20 K upon cooling (Fig. 1). For peak-type pyrrhotite, the λ-shaped peak was also reversed on the cooling ramp, but is accompanied by the production of a Weiss-type component, indicating that the peak-type has been partially converted into Weiss-type at high temperature (see the cooling curve and the 2nd run curves in Fig. 2). On the other hand, heating mixed-type pyrrhotite also gave rise to an increase of the Weiss-type component, and a decrease of the peak-type component as shown in Fig. 3. This feature suggests that the peak-type pyrrhotite (with the antiferromagnetic structure) has the same structure as the high-temperature form of the Weiss-type (with the ferrimagnetic ordering), and that this structure is maintained at least, in part, when a relatively fast cooling is performed.

When the samples were heated to temperatures higher than 550°C and subsequently cooled to room temperature, the magnetic behaviors were not recovered in any of the three types of pyrrhotite, however. If the heating process proceeds in a relative short term and the cooling is at a slow rate, the reversal of ferrimagnetization is possible. This loss of ferrimagnetism can be attributed to the decomposition of samples. At the highest experimental temperatures sulfur may evolve from the pyrrhotite samples so that the stoichiometry of the samples and accordingly the

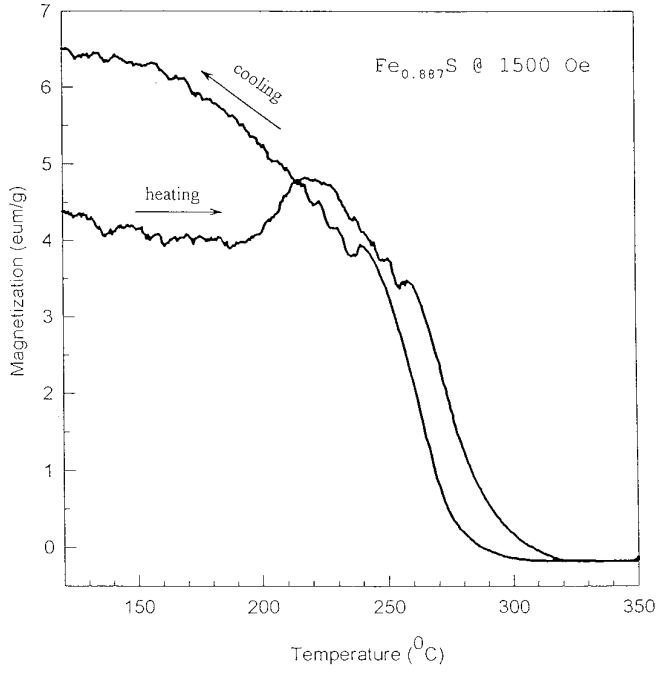

FIG. 3. Temperature dependence of magnetization for a mixed-type pyrrhotite.

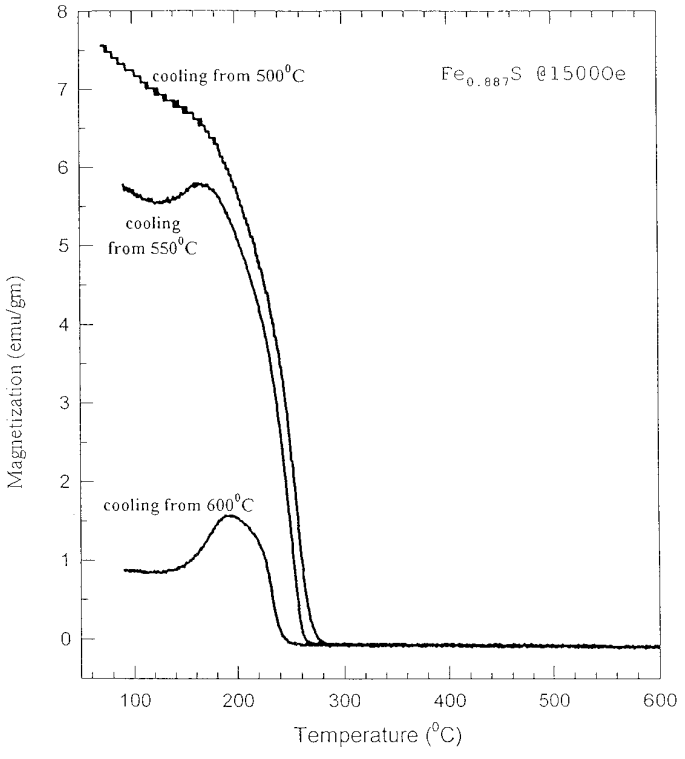

FIG. 4. The change of magnetization when the mixed-type pyrrhotite was cooled from different temperatures.

magnetic properties are altered. Figure 4 illustrates a magnetization measurement for mixed-type pyrrhotite, in which the sample was rapidly heated to 500, 550, or 600°C (in 10 min) and then slowly cooled to record its magnetization. It is interesting to notice that the mixed-type pyrrhotite can be transformed into pyrrhotite with more Weiss-type at 500°C, but with more peak-type at 550°C, and finally into almost complete peak-type at 600°C.

(3) Natural pyrrhotites. No matter from which ore separation processing stage the natural pyrrhotite was derived, the magnetization curves consistently showed all three transitions—anti-Curie, Curie transitions in pyrrhotite, and the Curie transition in magnetite (Fig. 5). It is not surprising that sample Inco 1 (magnetic portion) contains more Weiss-type component as well as magnetite, while sample Inco 2 (nonmagnetic portion) contains more antiferromagnetic component. The magnetization in all natural pyrrhotites was found to perish very easily upon heating the samples to 550°C. This is interpreted as related to the occurrence of impurities in the natural products which take over the excess sulfur from pyrrhotite at high temperature. It is noticed that the proportion of Weiss-type to peak-type pyrrhotite varies from the fast flotation samples (sample Inco 3) to the slow flotation sample (sample Inco 4). As seen later in the XRD observations, the change of magnetic type that has its origin in changes in the composition and structure results in the density order: Weiss-type > peak-type > nonmagnetic-type (mainly, antiferromagnetic-type). This may be important for the floating rate in separation process of the mineral.

3.2. DTA and HTXRD Results

In order to understand the magnetic behaviors illustrated above, DTA and HTXRD experiments were performed in two sequential heating-cooling cycles of 25–400°C and 25–600°C.

3.2.1. Weiss-type pyrrhotite. The ideal ordered structure for Fe_7S_8 as proposed by Bertaut is monoclinic (4). Its XRD pattern is characterized by significant peak splitting in the NiAs-type substructure diffraction (19). As shown in Fig. 6 this signature, especially on the $(102)_{NiAs}$ peak, was clearly manifested in natural magnetic sample (Inco 1) in spite of the presence of a number of weak peaks originating from impurity phases which cloud the superstructure reflections of pyrrhotites. Below and above these patterns are the calculated patterns for the 4*C* and 3*C* structure which are based on the structural information reported in the literature (18, 20). For the synthesized

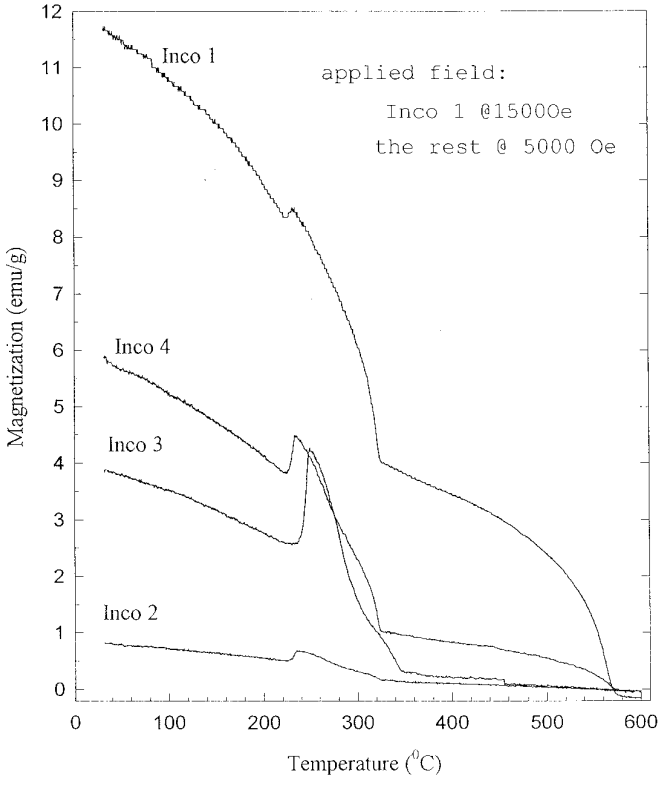

FIG. 5. Thermomagnetic curves for natural pyrrhotites provided by Inco. All the curves correspond to the heating process. Notice the magnetization contribution from magnetite which is characterized by its Curie transition at 580°C.

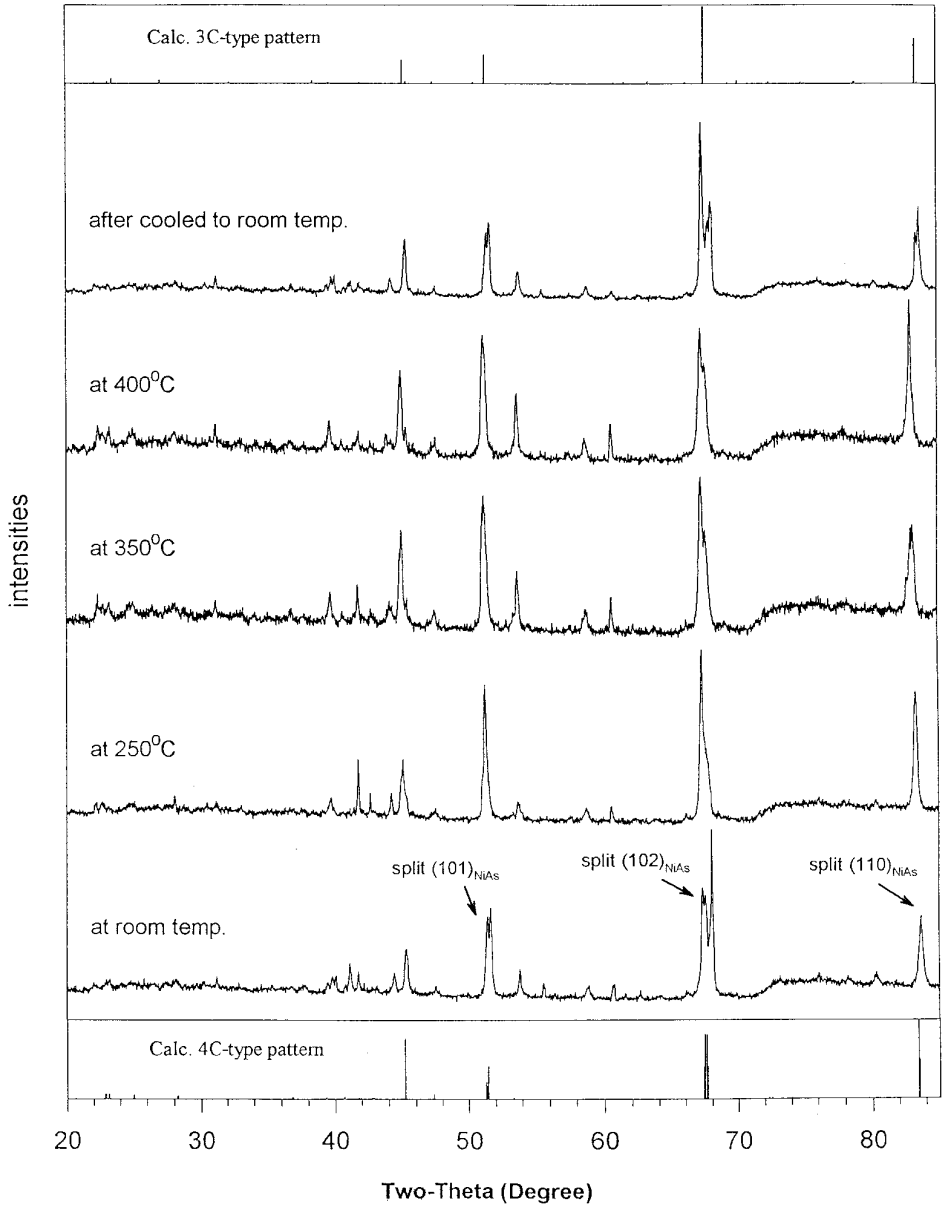

FIG. 6. HTXRD patterns for natural magnetic pyrrhotite (Inco1). Below and above are the calculated patterns for the 4*C* and 3*C* structures.

sample, however, this kind of splitting is not obvious even though a broadening of the peak can be recognized (see Fig. 7). At low angles (2θ), weak superstructure peaks can be identified and indexed according to the monoclinic structure, but they can as well be indexed as arising from the trigonal 3*c* superstructure because the powder XRD patterns of the two structure types are not strongly differentiated. Attempts to refine single-crystal diffraction from a synthetic Fe_7S_8 sample according to either the trigonal or monoclinic structure were unsuccessful. When diffuse diffraction between any two integer l reflections in the reciprocal space of the NiAs subcell was scanned, weak diffuse reflections were observed at $l = 1/3$ and 2/3 implying a 3*C* supercell, and also at $l = 1/4$, 1/2, and 3/4 implying a 4*C* supercell (see Fig. 8). This evidence indicates that the synthetic sample at this resolution yields not single crystals, but regions with mixed stacking sequences. A bulk sample contains stacking faults leading to different regions of 4*C* stackings (*ABCD*, *BACD*, *CABD*, and so on) such that the monoclinic symmetry is lost in the X-ray averaging. At the single crystal level, on the other hand, electron diffraction yields evidence of partially ordered ''monoclinic'' structures.

When the natural occurring Fe_7S_8 sample (Inco1) was

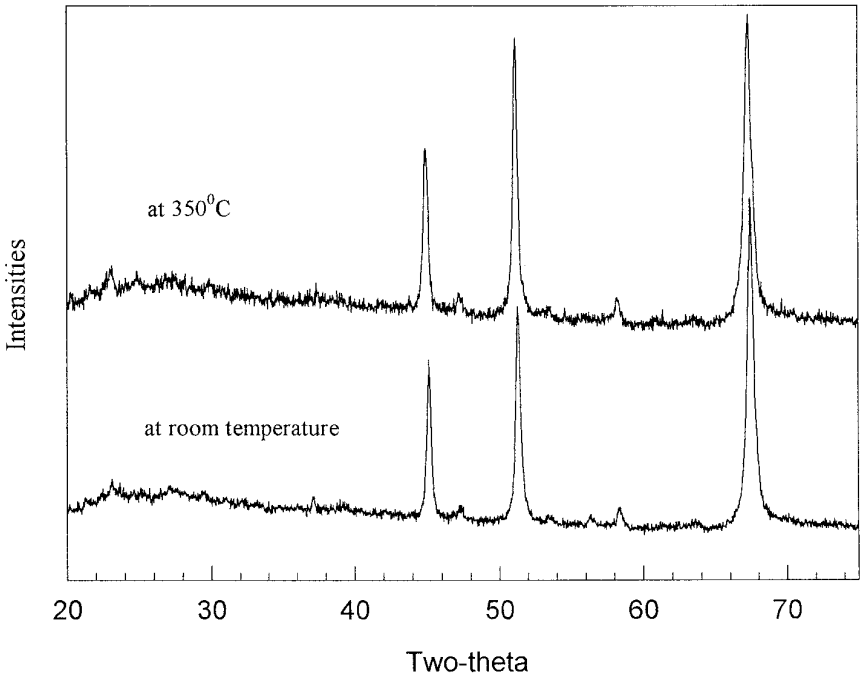

FIG. 7. HTXRD patterns for the synthetic Fe_7S_8 sample.

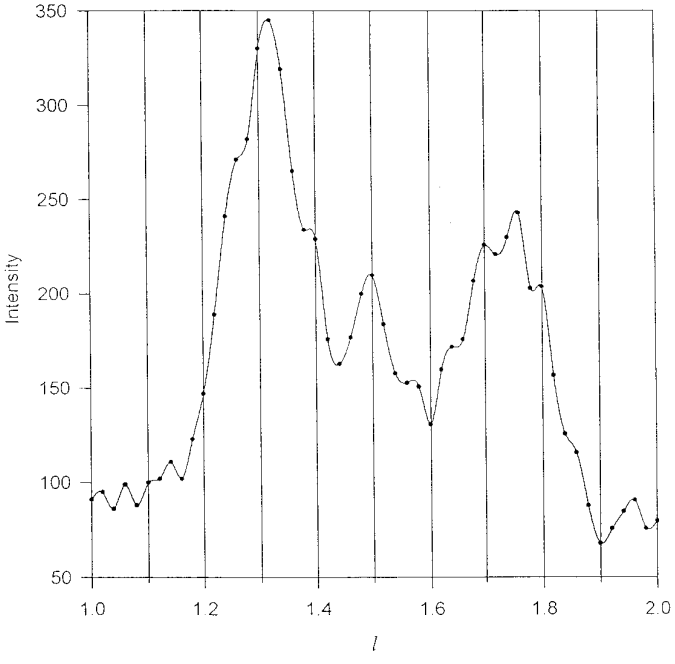

FIG. 8. The X-ray diffuse diffraction scanned between indices (031) and (032) of NiAs-type cell. Notice that reflection maxima approximately appear at 1/4, 1/3, 1/2, 2/3, and 3/4 of integral *l*.

heated to 150–250°C, the split peaks in the XRD pattern were clearly seen to converge, and then a diffraction pattern closely approximating that expected from the trigonal structure was formed (Fig. 6). When the temperature was raised between 300 and 400°C, the peaks showed a small splitting. This is probably due to interactions between the pyrrhotite phase and impurity phases at high temperature. The monoclinic pattern was recovered on cooling to room temperature. The intensity changes in the split $(102)_{NiAs}$ and $(110)_{NiAs}$ peaks with the change of temperature suggest that the heating cycle led to the different intra- and/or interlayer ordering in the sample. This observation supports the transition sequence proposed for this type of pyrrhotite in a previous study (1). On the other hand, the synthetic samples do not show a significant change in the XRD patterns until 550°C. This lack of differentiation results from the similarity in the patterns for the monoclinic and the trigonal structures and the greater extent of disorder relative to the natural samples.

When the temperature exceeded 550°C, a loss of sulfur from the synthetic sample was indicated by the resultant modification of the XRD patterns (see Fig. 9). Initially at 550°C, almost all the substructure diffraction peaks showed some splitting with time, indicative of sulfur loss relative to the original 7:8 ratio. As the sample was kept in the temperature range between 550 and 600°C, the split peaks converged, and finally transformed into a nearly ideal NiAs-type pattern with the disappearance of superstruc-

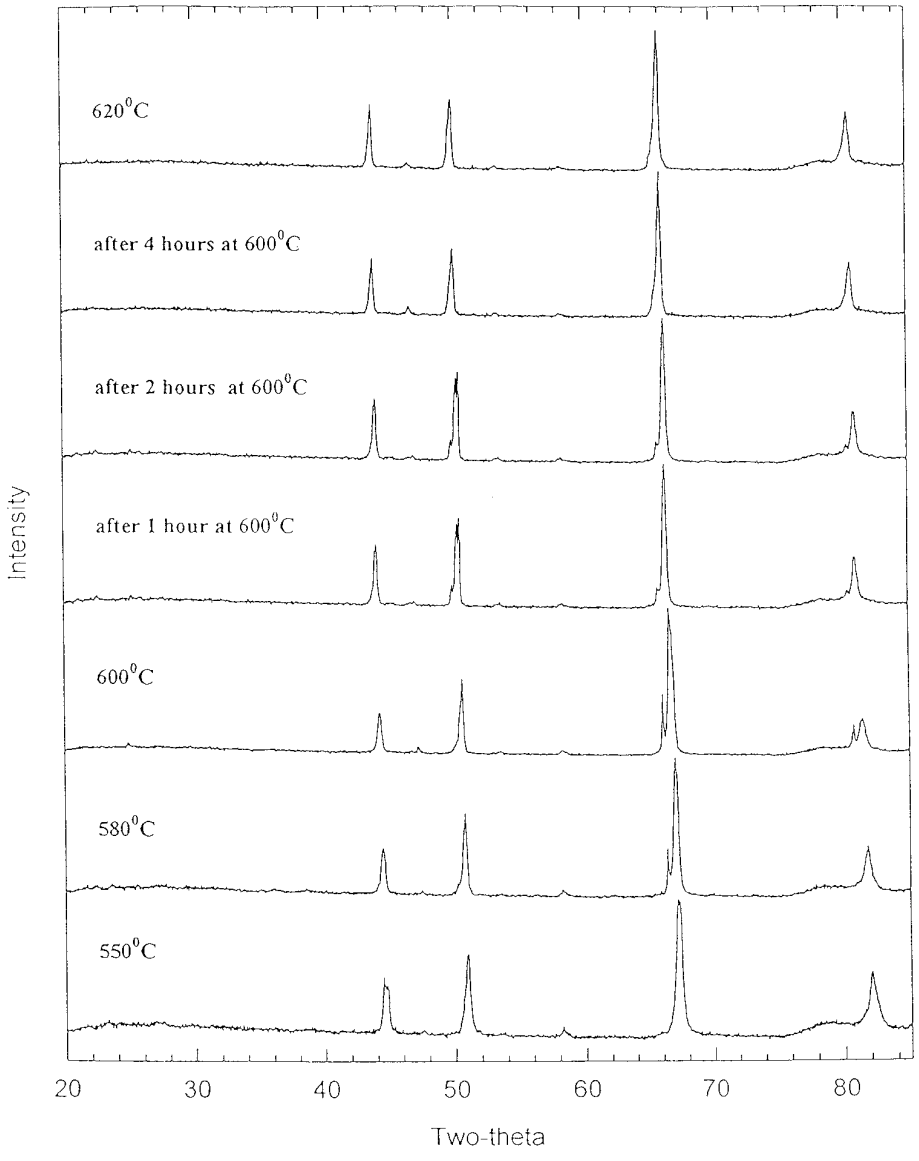

FIG. 9. HTXRD patterns of the synthetic Fe_7S_8 sample for $T > 550$°C.

ture peaks at low angles. For the natural pyrrhotite samples, because chemical reactions between the pyrrhotite and impurities may occur, it is difficult to identify the decomposition process by XRD patterns. Since the samples cooled from 600°C have been found to show no ferrimagnetism, the loss of ferrimagnetism can be attributed to the loss of sulfur (and hence of vacancies) accompanied by a disordering of the vacancies (i.e., all sites equally occupied) at high temperature, and inadequate time for ordering during cooling. On the other hand, there is a noticeable volume expansion of the unit cell from Fe_7S_8 to FeS in excess of the background thermal expansion. Therefore, the change in XRD pattern with time at $T >$ 550°C was such that a set of diffraction lines corresponding to the larger cell parameters appeared and eventually replaced the original pattern, which corresponded to the smaller cell and thus the simple NiAs structure was observed to grow through loss of sulfur above about 550°C.

A large peak was clearly observed on the DTA curves for both the natural and synthesized samples (see Fig. 10 and 11) at the temperatures at which the Curie transition is known to occur: at 315°C on the heating ramp and at 305°C on the cooling ramp, provided that the sample was not heated to a temperature at which noticeable decomposition occurred. In addition, a small thermal anomaly was identified at temperatures between 200 and 240°C. This

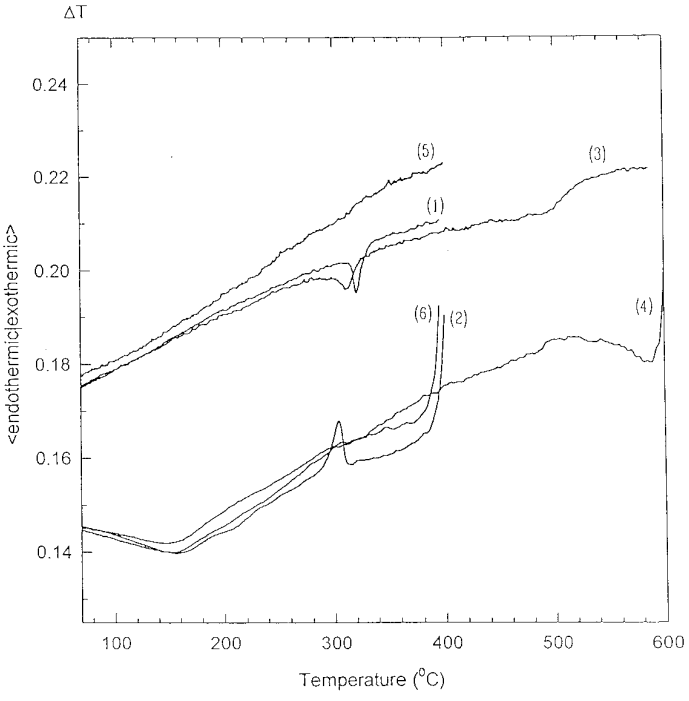

FIG. 10. DTA curves of the natural magnetic pyrrhotite (Inco1) subjected to three sequential heating–cooling cycles: curve 1, heating from 50 to 400°C; curve 2, cooling from 400 to 50°C; curve 3, heating from 50 to 600°C; curve 4, cooling from 600 to 50°C; curve 5, heating from 50 to 400°C; curve 6, cooling from 400 to 50°C.

thermal anomaly was reversed when the samples were cooled from 400°C. The whole process was repeated in a subsequent heating up to 600°C. However, only a small peak at 305°C and a wide kink at 260°C were observed when the samples were cooled from the temperature of 620°C. These DTA observations are consistent with the thermomagnetic and HTXRD observations. The small anomaly at temperatures between 200 and 240°C, as interpreted in the previous report (1), results from the tendency to order from the *ABCD* 4*C* structure to *ABC* 3*C* structure and vice versa. Although the large peak can be attributed to the Curie transition, its intensity and the decrease of intensity brought about by heating up to 620°C are particularly worthy of notice. Since the ordering of magnetic spins is essentially independent of composition, the small peak at about 310°C on the DTA curve 4 (cooling from 600°C) as shown in Figs. 10 and 11 is considered to represent a ''net'' spin order–disorder process. This kind of small thermal anomaly also appeared in the DTA experiments for other samples, such as the antiferromagnetic FeS sample reported earlier (2) and the peak-type $Fe_{1-x}S$ sample as shown later. Hence it is concluded that the unusual intensity found at 300–320°C for the Fe_7S_8 sample results from significant contributions from vacancy disordering. Since TEM observations have shown that the disordering of vacancies has developed to a significant extent by 340°C, it can be concluded that this intense thermal anomaly corresponds to a transition for which the disordering of spins is associated with the disordering of vacancies. Once the vacancies have been removed from the lattice, or if the vacancies remain disordered such that adjacent planes are equivalent, the ordering of magnetic spins will proceed as a pure spin ordering.

3.2.2 Peak-type pyrrhotite. Figure 12 shows the DTA curves obtained from three sequential heating–cooling cycles for the $Fe_{0.906}S$ pyrrhotite showing the peak-type magnetic anomaly. A small peak invariably appeared at 315°C on heating curves and at 305°C on cooling curves. This peak corresponds to the magnetic moment order–disorder transition (Néel point), and, as expected, it is not affected by the ultimate heating temperature. In addition, curves 1 (from 50 to 400°C), 2 (from 400 to 50°C), and 3 (from 50 to 600°C) show a thermal anomaly at temperatures between 230 and 280°C (pointed to by down arrows); while curves 4 (from 600 to 50°C), 5 (a subsequent second run from 50 to 400°C), and 6 (a subsequent second run from 400 to 50°C) show an anomaly at temperatures between 200 and 180°C (pointed to by up arrows). It appears that

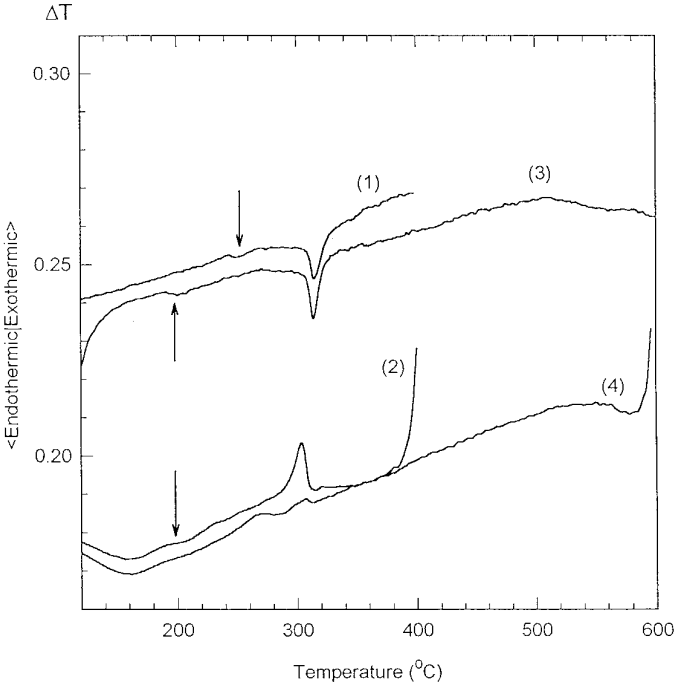

FIG. 11. DTA curves of the synthetic Fe_7S_8 sample subjected to two sequential heating–cooling cycles: curve 1, heating from 50 to 400°C; curve 2, cooling from 400 to 50°C; curve 3, heating from 50 to 600°C; curve 4, cooling from 600 to 50°C. The small anomalies are indicated by arrows.

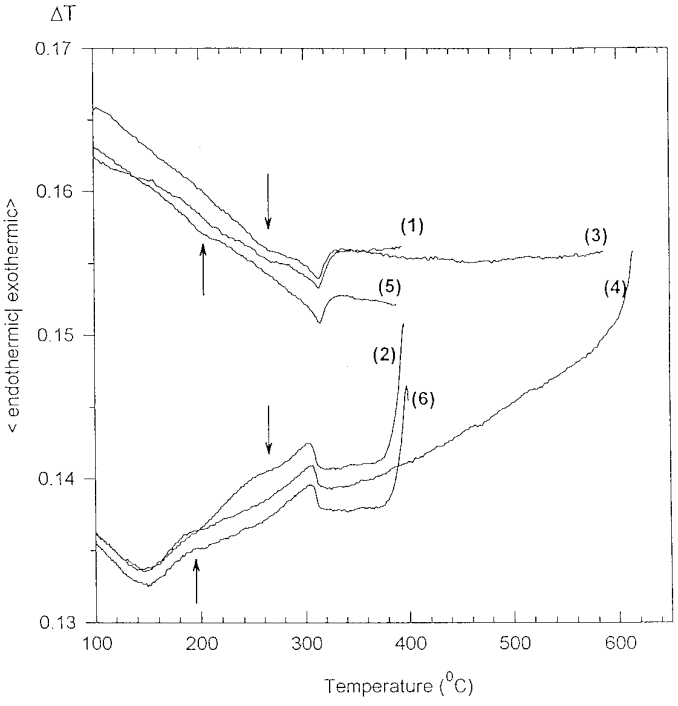

FIG. 12. DTA curves of the peak-type sample ($Fe_{0.906}S$) subjected to three sequential heating–cooling cycles (5 K/min under Ar-gas flow): (1) heating from 50 to 400°C; (2) cooling from 400 to 50°C; (3) heating from 50 to 600°C; (4) cooling from 600 to 50°C; (5) heating from 50 to 400°C; (6), cooling from 400 to 50°C. The arrows indicate small anomalies.

the former (between 230 and 280°C) corresponds to the anti-Curie transition, while for the latter, observed at temperature lower than 200°C, it is suggested that this transition has been modified, probably as a result of change in the composition at 600°C. These results indicate that all the transition processes in this type of pyrrhotite, except the spin disordering, have relatively low integral enthalpy changes.

Since peak-type pyrrhotite occurs in the composition region in which the various *NC* ($N = 5$, 6 and 11) superstructures were discovered, XRD patterns were examined to determine whether an *NC* structure could be identified in the synthetic sample. As can be seen in Fig. 13, several superstructure diffractions can be recognized in the low angle region along with the NiAs-type substructure reflections. Three relatively intense peaks (they will be named peak 1, peak 2, and peak 3, and indicated by arrows in Fig. 13) correspond to $d = 5.85$ Å (at 22.56°), $d = 6.14$ Å (21.48°), and $d = 6.79$ Å (19.40°), respectively. Based on the XRD information reported in the literature (21), the room-temperature pattern for the $Fe_{0.906}S$ sample seems to fit the reported $5C$ superstructure quite well, though $6C$ and $11C$ may be possible due to their very similar diffraction patterns and the limited diffraction evidence. Furthermore, the subcell parameters $a = 3.447$ Å and $c = 5.742$ Å were calculated from the substructure diffractions. Consequently, peaks 1($d = 5.85$ Å) and 2 ($d = 6.14$ Å) can be indexed as diffractions $(101)_{5c}$ and $(100)_{5c}$ for the $2A \times 2A \times 5C$ hexagonal superstructure. However peak 3 ($d = 6.79$ Å) cannot be indexed by any known superstructure type. It is hence proposed that this reflection arises from superstructure that is not integral in *c*. Based upon the TEM results for Fe_7S_8 (1), it is not expected that long-range ordering will be established in the pyrrhotites over the experimental annealing times. For the synthetic samples intergrowth of various stacking sequences inevitably appears, and an incommensurate structure with a nonintegral *c* results. Therefore, the ideal *NC* structure will occur only in domains along with disordered regions and other variants.

In order to relate magnetic properties in peak-type pyrrhotite with vacancy ordering it is necessary to determine the magnetic structure consistent with a given *NC* structure. First of all, consider the stacking sequences in the experimentally confirmed *NC* superstructures. The commonly accepted stacking patterns are illustrated in Fig. 14 (22–24). In these stacking patterns, it is particularly important that the *NC* structures ($N = 5$, 6, or 11) occur only with the *ABCD* stacking sequence, as in the well-known monoclinic Fe_7S_8 case, and that if we assume that, as is true for Fe_7S_8, the adjacent iron layers are antiferromagnetically coupled, none of these stacking patterns yields a net ferrimagnetic structure (see column 2 of Fig. 14). Thus the known *NC* structures are inconsistent with ferrimagnetic ordering of the type found in Fe_7S_8.

Furthermore, a closer inspection of the HTXRD patterns reveals that with increasing temperature the substructure reflections showed no significant change in intensity, but the signature peaks for the $2A \times 2A \times 5C$ superstructure (peaks 1 and 2) were found to disappear over the temperature range 150–200°C, then to reappear after the temperature reached to 250°C, and remain until the temperature was above 350°C (Fig. 13). In addition, the reversal behavior in XRD patterns upon heating and cooling is consistent with what was observed in the thermomagnetic and DTA experiments; i.e., when the ultimate heating temperature was lower than 400°C, the original diffraction pattern was exactly recovered, while heating to temperatures higher than 550°C resulted in a high-temperature pattern analogous to that of the NiAs-type structure. Another observation is that peak 3 which, as suggested above, is associated with nonintegral *c* shifts toward high angle (2θ) with an increase of temperature, indicating a tendency for the structure to transform toward increase of domain size with increasing temperature.

In order to interpret the behavior observed in the diffractions of the *NC* structure in accordance with the anti-Curie

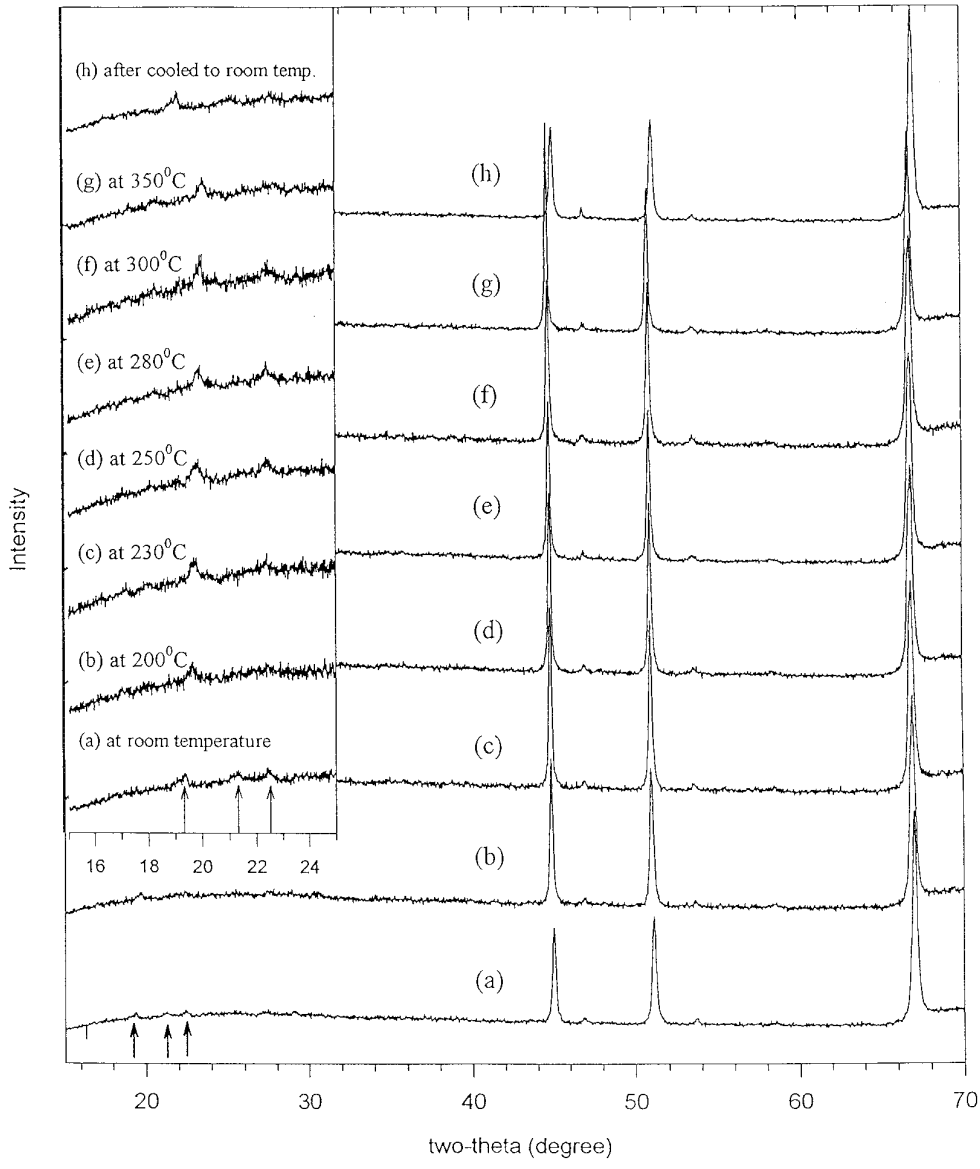

FIG. 13. HTXRD patterns of the sample $Fe_{0.906}S$ (peak-type). The inset is the low-angle region with an enlarged scale. The superstructure peaks are arrowed.

magnetic behavior, we appeal to the transition sequence model that was proposed for the case of Weiss-type. It is thus suggested that peak-type pyrrhotite with an *NC* structure has an order–disorder transition sequence similar to Weiss-type, that is, *ABCD* stacking → *ABC* stacking → *DFDFDF* stacking → disordering. It is convenient for this discussion to name the *ABCD* and *ABC* stackings as *K–F* stacking, namely, stacking of alternating Kagome nets and filled layers, and name the alternate stacking of disordered partially occupied layers and filled layers as *D–F* stacking. A *D–F* stacking sequence arising from an antiferromagnetic parent *K–F* stacking is also antiferromagnetic (see Fig. 14). Hence, because *ABC* stacking is not commensurate with the *NC* structures, if *ABC* stacking (or mixed stacking) occurs as an intermediate phase during the vacancy order–disorder transition over the temperature range 150–250°C, the compensation of magnetic moments between ordered and filled layers in an *NC* structure is broken. Thus the growth of *ABC* layering leads to an increase of ferrimagnetization which is followed by a decrease in the magnetization with the growth of *D–F* layering. In XRD it was observed that the 5*C* superstructure was lost during the *ABC* layering or mixed layering, and was reformed in the *D–F* layered structure which restored

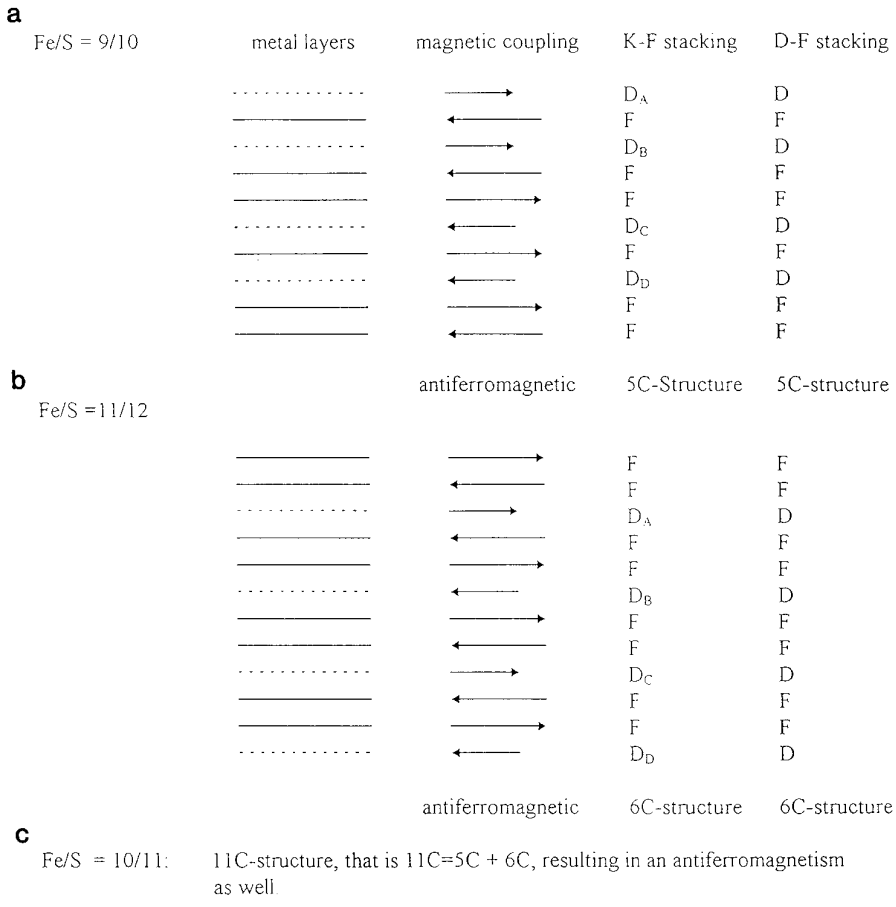

FIG. 14. Schematic representation of layering patterns and magnetic coupling for intermediate pyrrhotites with *NC* structures. D_A, the *A*-Kagome net, and so on; *D*, disordered partially occupied layer; *F*, the iron-filled layer.

the *C* modulation. Thus, the following transition sequence is proposed for the peak-type pyrrhotite:

$$K\text{–}F \text{ stacking } (ABCD) \rightarrow K\text{–}F \text{ stacking } (ABC + ABCD) \rightarrow D\text{–}F \text{ stacking.}$$
(antiferromagnetic) (ferrimagnetic) (antiferromagnetic)

The disordered structure between the *K–F* stacking and *D–F* stacking is ferrimagnetic, giving rise to the observed anti-Curie transition. Furthermore, in the cooling direction, the incommensurate structure with mixed *K–F* stackings follows the *D–F* stacking structure and develops ferrimagnetism at the λ point (not at the Curie point). However, as the temperature is further decreased, a part of the pyrrhotite with the disordered stacking sequences may not have transformed into regular *K–F* stacking with ordering of the vacancies within the layers. As result, this portion of the pyrrhotite remains as Weiss-type.

4. CONCLUSIONS

We have conducted a study on the relationship between the thermomagnetic properties and structure transitions in pyrrhotites. The results have been interpreted in terms of the known idealized structures in which the vacancies order such as to form the Kagome nets and Kagome nets tend to stack as the *ABCD* sequence at low temperature. For Fe_7S_8, HTXRD experiments reveal that natural magnetic pyrrhotite can form a stable monoclinic-type structure and follow the previously proposed transition sequence very well. At the Curie transition temperature, this pyrrhotite shows an extraordinarily intense DTA peak, implying a structural modification that is related to the disordering of magnetic spins. As for the so-called peak-type pyrrhotite with compositions over the range Fe_9S_{10}–$Fe_{11}S_{12}$, the ideal *ABCD* stacking of Kagome nets results in part in *NC* structures ($N = 5$, 6, or 11). As the *ABCD* stacking transforms to mixed stacking with *ABC* components, the *NC* structure is lost, and along with the accompanying stacking disorder comes a ferrimagnetic contribu-

tion from the uncompensated spins in the layers. When the vacancies disorder within the layers to form *D–F* stacking the *NC* period is regained, and along with this periodicity comes antiferromagnetic ordering.

ACKNOWLEDGMENTS

We express our sincere thanks to Dr. Alfred Kracher for the EMP analysis work, to Mr. Kevin Dennis for generous assistance with the thermomagnetic and DTA measurements, and to Mr. Hengning Wu and Mr. Larry Margulies for their help in the DTA experiments. We appreciate a generous gift of Cr-anode provided by Inco Limited, Canada. Their support is very important. This research was also supported by the Office of the Basic Energy Sciences, through Materials Sciences Division, Ames Laboratory—operated for the U.S. Department of Energy by Iowa State University under Contract W-7405-Eng-82.

REFERENCES

1. F. Li and H. F. Franzen, a paper submitted along with this paper.
2. F. Li and H. F. Franzen, submitted for publication (1996).
3. C. B. van den Berg, *Ferroelectics* **4,** 103–116 and 195–212 (1972).
4. E. F. Bertaut, *Bull. Soc. Fr. Mineral. Cristallogr.* **79,** 276 (1956).
5. R. H. Carpenter and G. A. Desborough, *Am. Mineral.* **49,** 1350 (1964).
6. M. E. Fleet, and N. MacRae, *Can. Mineral.* **9,** 699 (1969).
7. N. Morimoto, H. Nakazawa, K. Nishiguchi, and M. Tokonami, *Science* **168,** 964 (1970).
8. A. Vorma, *Bull. Geol. Soc. Finland* **42,** 3 (1970).
9. K. Hayase, R. Otsuka, and T. Mariko, *Mineralog. J.* **4,** 41 (1963).
10. F. K. Lotgering, *Z. Phys. Chem* **4,** 238 (1955).
11. F. K. Lotgering, *Phillips Res. Rep.* **11,** 190 (1956).
12. J. T. Sparks, W. Mead, A. J. Kirschbaum, and W. Marshall, *J. App. Phys.* **31,** 356S (1960).
13. A. E. Andersen and P. Torbo, *Acta Chem. Scand.* **21,** 2841 (1967).
14. T. Hirone and N. Tsuya, *Phys. Rev.* **83,** 1063 (1951).
15. T. Hirone, S. Maeda, and N. Tsuya, *J. Phys. Soc. Jpn.* **9,** 736 (1954).
16. M. G. Townsend, A. H. Webster, and J. L. Horwood, *J. Phys. Chem. Solids* **40,** 183 (1979).
17. E. J. Schwarz and D. J. Vaughan, *J. Geomag. Geoelectr.* **24,** 441 (1972).
18. M. Tokonami, K. Nishiguchi, and N. Morimoto, *Am. Mineral.* **57,** 1066 (1972).
19. D. J. Vaughan and J. R. Craig, ''Mineral Chemistry of Metal Sulfides,'' Cambridge Univ. Press, 1978.
20. M. E. Fleet, *Acta Crystallogr. B* **27,** 1864 (1971).
21. JCPDS-ICDD (1992): 29–724, 29–725, and 29–726.
22. K. Koto, N. Morimoto, and A. Gyobu, *Acta Crystallogr. B* **31,** 2759 (1975).
23. K. Koto and M. Kitamura, *Acta Crystallogr. A* **37,** 301 (1981).
24. I. Dodony and M. Posfai, *Eur. J. Mineral.* **2,** 529 (1990).